

# Ponderomotive processes as proxies for breaking of ion acoustic solitary waves

Amar Kakad<sup>a)</sup> and Bharati Kakad<sup>b)</sup>

Indian Institute of Geomagnetism, New Panvel, Navi Mumbai 410218, India

(Received 23 August 2016; accepted 10 November 2016; published online 1 December 2016)

Wave breaking is a ubiquitous nonlinear phenomenon in plasma that is followed by sudden drop of wave amplitude after a wave steepening. We perform fluid simulation of the ion acoustic solitary waves (IASWs) to investigate the start time of the wave steepening and breaking process. This simulation demonstrates that a long wavelength perturbation in the electron and ion equilibrium densities evolves into two long wavelength IASWs. These IASWs steepen and break into short wavelength solitary structures, which become stable ion acoustic solitons at later time. From the detailed analysis of simulation output, we accomplish the criteria for steepening and breaking of the IASWs based on the (a) acceleration of IASWs (b) balance between maximum potential energy and the maximum electron kinetic energy. Furthermore, we examined the ponderomotive potential and the ponderomotive frequency of the electrons and ions during the process of the generation, steepening and breaking of these IASWs. It is observed that the maximum ponderomotive potential of both electrons and ions enhances during the steepening and attains the maximum close to the breaking of the IASWs. The simulation shows that the electron (ion) average ponderomotive frequency is considerably higher than the electron plasma frequency in the initial phase of generation of IASWs, which rapidly oscillates and approaches to frequencies much smaller than electron (ion) plasma frequency. These ponderomotive frequencies remain unchanged until the start of steepening of the IASWs; however, both frequencies are found to increase during the steepening and breaking of these IASWs. Based on this information, we propose that the ponderomotive potential and ponderomotive frequencies of electrons and ions can be used as proxies to determine the steepening and breaking time of the IASWs. We find that the onset time of the wave breaking varies inversely with the thermal velocity of the electrons and the amplitude of the initial density perturbation (IDP), while it is directly proportional to the width of the IDP. It is also noted that the number of solitons formed in the system and their characteristics depends on the electron temperature, width, and amplitude of the IDP. *Published by AIP Publishing.*

[<http://dx.doi.org/10.1063/1.4968842>]

## I. INTRODUCTION

The nonlinear propagation of waves in plasma has a fundamental limitation given by the wave breaking threshold. Dawson<sup>1</sup> introduced the concept of wave breaking in a cold homogeneous plasma to describe the limiting amplitude of the electron plasma waves/oscillations in non-relativistic plasma. The author showed that the wave breaking in a cold plasma occurs when elements of the plasma electron fluid that started out in different positions overtake each other, while moving back and forth during the passage of the wave. For non-relativistic plasmas, this overtaking happens when the peak fluid velocity equals the phase speed of the plasma wave.<sup>1</sup>

Studies on the breaking of large amplitude electron plasma waves/oscillations in cold homogeneous<sup>1</sup> and thermal<sup>2-5</sup> non-relativistic plasmas have been carried out by a number of researchers. In a warm plasma, the plasma temperature plays a significant role in determining the wave breaking amplitude.<sup>2-4</sup> Coffey<sup>2</sup> proposed the correction

accounting for the thermal effects by using one-dimensional waterbag model which is equivalent to a warm-fluid model. The author derived an analytical expression for the maximum wave amplitude as a function of the electron temperature, which shows that the thermal effects significantly reduce the wave breaking limit for electron plasma wave.

In this paper, we investigate the steepening and breaking of the ion acoustic solitary waves (IASWs) in collisionless unmagnetized electron-ion plasma fluid system. There are few studies that have addressed the criteria of the breaking of ion acoustic (IA) waves in plasmas<sup>6-9</sup> earlier. Judice<sup>7</sup> proposed an approximate criterion for the breaking of ion acoustic wave in plasma. The author showed that the ion acoustic wave breaks when ion trapping velocity  $(e\phi/m_i)^{1/2}$ , exceeds the phase velocity of the wave  $\omega/k = c_s$ , where  $\phi$  is the wave potential,  $m_i$  is the ion mass,  $\omega$  and  $k$  are the frequency and wave number of the wave, and  $c_s$  is the ion acoustic velocity. Recently, using fluid simulations, it is shown that the initial large wavelength perturbations in the electron and ion densities evolves into the chains of the ion acoustic (IA) solitons through wave breaking process in plasma.<sup>10</sup>

In this paper, we investigate the nonlinear evolution of the IASWs up to and beyond their wave breaking limit. Our

<sup>a)</sup>amar@iigs.iigm.res.in

<sup>b)</sup>ebharati@iigs.iigm.res.in

aim is to understand the response of the ponderomotive processes in the generation, steepening and breaking of the IASWs. We have investigated the generation and evolution of IASWs in detail and estimated their breaking and steepening time. The role of electron temperature and characteristics of initial density perturbation (IDP) in the determining time of IASW steepening and breaking is examined. In Section II, we present the fluid simulation model. Generation of IASWs and their breaking is discussed in Section III. The ponderomotive processes involved in the process of steepening and breaking of the IASWs are discussed in Section IV. The role of electron temperature on the steepening and breaking of the IASWs is discussed in Section V. Section VI describes the time dependency of the IASW breaking and steepening on the amplitude and width of the IDP. The results are concluded in section VII.

## II. SIMULATION MODEL

We consider a homogeneous, collisionless two-component plasma consisting of fluid electrons and fluid ions ( $H^+$  ions). For the nonlinear ion acoustic (IA) waves propagating parallel to the magnetic field, the dynamics of the electrons and ions is governed by the multi-fluid equations of continuity, momentum, and energy of each species, and the Poisson equation<sup>10</sup> as follows:

$$\frac{\partial n_j}{\partial t} + \frac{\partial(n_j v_j)}{\partial x} = 0, \quad (1)$$

$$\frac{\partial v_j}{\partial t} + v_j \frac{\partial v_j}{\partial x} + \frac{1}{\mu_j n_j} \frac{\partial P_j}{\partial x} - \frac{Z_j}{\mu_j} E = 0, \quad (2)$$

$$\frac{\partial P_j}{\partial t} + v_j \frac{\partial P_j}{\partial x} + \gamma_j P_j \frac{\partial v_j}{\partial x} = 0, \quad (3)$$

$$\frac{\partial E}{\partial x} = n_i - n_e. \quad (4)$$

The electric field ( $E$ ) in the above set of equations can be written in terms of an electrostatic potential ( $\phi$ ) with the relation  $E = -\partial\phi/\partial x$ . In the equations listed above, the subscripts  $j=e$  and  $i$  are, respectively, used for electrons and ions. The variables  $n_j$ ,  $P_j$ , and  $v_j$  are plasma density, pressure, and velocity of the species  $j$ , respectively. Here,  $\mu_j = m_j/m_i$ , where  $m_j$  and  $Z_j$ , respectively, represent the mass and charge of the  $j$ th species (i.e.,  $Z_e = -e$  for electron and  $Z_i = e$  for ions). Further, densities are normalized with the background ion density  $n_{i0}$ , velocities with the ion thermal velocity  $C_i = (T_i/m_i)^{1/2}$ , time with the inverse of ion plasma frequency  $\omega_{pi}^{-1}$ , length with the ion Debye length, electric field  $E$  with  $T_i/e\lambda_{di}$ , and thermal pressures  $P_j$  with  $n_0 T_i$ . Here,  $n_{i0} = n_{e0} = n_0$ ,  $\omega_{pi} = \sqrt{n_0 e^2 / \epsilon_0 m_i}$  and  $\lambda_{di} = \sqrt{\epsilon_0 T_i / n_0 e^2}$ . We assume the same adiabatic index, that is,  $\gamma_j = 3$ , for both species in the equation of state given by Equation (3).

In the simulation code, the spatial derivatives of the quantities in Equations (1)–(4) are computed using the finite difference scheme,<sup>10–17</sup> which is accurate to the fourth order. We integrate Equations (1)–(3) in time by the leap-frog method,<sup>10,12–17</sup> which is accurate to the second order. The

leap-frog method gives rise to a grid separation numerical instability. To eliminate small wavelength modes linked with such numerical instability, we have used a compensated filter.<sup>10,12–17</sup> A necessary condition for the convergence of the explicit finite difference method used in our simulation is that, it is constrained by the Courant-Friedrichs-Lewy (CFL) or Courant condition,  $V_{max} \frac{\Delta t}{\Delta x} \leq 1$ . This condition simply states that for any given time-step, the maximum velocity in the system ( $V_{max}$ ) must not be greater than that which would allow fluid to travel more than one grid-step. Simulations where the Courant number exceeds one, generally become unstable and quickly blow up, for example, values grow rapidly and uncontrollably. Often, these problematic simulations may sometimes run successfully by reducing the time-step, with the concomitant increase in computing time. The  $\Delta x$  and  $\Delta t$  in the present simulation are chosen in such a way that the Courant condition is always fulfilled.

One of the main objectives of this study is to obtain the accurate wave breaking condition. To analyse the exact time step of the wave breaking, we have to save simulation output at a very small time step, which increases the data size. Further, this upsurges the computational time to reach to the exact time step at which the wave breaking occurs. Therefore, to reduce the computational time in obtaining the precise wave breaking condition, we considered the electron to ion mass ratio,  $m_e/m_i = 0.01$  in the simulation.

We perform the fluid simulations in one-dimensional system with the periodic boundary conditions. For all simulation runs, we assume an artificial electron to ion mass ratio  $m_e/m_i = 0.01$  and the electrons are hotter than the ions. The flow velocities of the electrons and the ions at  $\omega_{pi} t = 0$  are assumed to be zero initially, that is,  $v_e(x) = v_i(x) = 0$ . The background electron and ion densities are set to one, that is,  $n_{e0} = n_{i0} = n_0 = 1$  and  $\omega_{pe} = 10\omega_{pi}$ . As an initial condition, we used the localized perturbation (IDP) in the equilibrium electron and ion densities given by

$$\delta n = \Delta n \operatorname{sech}^2 \left[ \frac{(x - x_c)}{l_0} \right]. \quad (5)$$

In the equation above,  $\Delta n$  and  $l_0$  are the amplitude and width of the superimposed IDP. Here,  $x_c$  is the center of the simulation system. Thus, the perturbed densities  $n_j(x) = n_{j0} + \delta n$  takes the following form as the initial condition

$$n_j(x) = n_{j0} + \Delta n \operatorname{sech}^2 \left[ \frac{(x - x_c)}{l_0} \right]. \quad (6)$$

We perform fluid simulations for different parameters given in Tables I and II. In a first, the electron temperature is varied in the range of  $4-15T_i$  that corresponds to electron thermal speed  $V_{th|e} = 20-38.7 V_{th|i}$ . For these simulation runs, we chose fixed IDP amplitude  $\Delta n = 0.5n_0$  and the width  $l_0 = 100\lambda_{di}$ . Details of these simulation runs with their corresponding parameters are given in Table I and they are used to investigate the effects of electron temperature on IASW breaking. Second, we selected two electron temperatures (i)  $T_e = 4T_i$  and (ii)  $T_e = 10T_i$ , and varied IDP width between

TABLE I. Parameters used in the simulation runs to investigate the effect of electron temperature on the onset time of the steepening and breaking of the IASWs.

Run	$T_e$ [ $T_i$ ]	$V_{th e}$ [ $V_{th i}$ ]	$dx$ [ $\lambda_{di}$ ]	$dt$ [ $\omega_{pi}^{-1}$ ]	$L_x$ [ $\lambda_{di}$ ]	$l_0$ [ $\lambda_{di}$ ]	$\Delta n$ [ $n_0$ ]	$t_S$ [ $\omega_{pi}^{-1}$ ]	$t_B$ [ $\omega_{pi}^{-1}$ ]	$N_{sol}$
1	4	20	0.4	$10 \times 10^{-4}$	$3 \times 10^5$	150	0.5	296	528	8
2	6	24.5	0.4	$9 \times 10^{-4}$	$3 \times 10^5$	150	0.5	230	446	7
3	8	28.3	0.4	$7 \times 10^{-4}$	$3 \times 10^5$	150	0.5	196	392	6
4	10	31.6	0.4	$6 \times 10^{-4}$	$3 \times 10^5$	150	0.5	160	355	5
5	12	34.6	0.4	$5 \times 10^{-4}$	$4 \times 10^5$	150	0.5	136	324	4
6	15	38.7	0.4	$4 \times 10^{-4}$	$3 \times 10^5$	150	0.5	118	292	4

$l_0 = 100 - 200\lambda_{di}$ , and IDP amplitude in the range of  $\Delta n = 0.5 - 1n_0$  to examine the role of IDP in the steepening and breaking of IASWs in plasma. These parameters are mentioned in Table II. It should be noted that the width of the IDPs are chosen in such a way that it satisfies the required criteria of the long wavelength (i.e.,  $k^2\lambda_{de}^2 \ll 1$ ) as suggested by Kakad *et al.*<sup>10</sup>

### III. FORMATION AND BREAKING OF THE IASWS

We first undertake a discussion of the generation and evolution of IA solitons; when the long wavelength IDP is used to perturb the background electron and ion densities in the fluid simulation. In a plasma with no applied magnetic field, the wave phenomena are particularly simple because such a plasma has only two electrostatic normal modes, namely, a high and a low frequency mode. The high-frequency mode is one in which the electrons oscillate rapidly about stationary

TABLE II. Parameters used in the simulation to investigate the effect of the width and amplitude of the IDP on the steepening and breaking of the IASWs. In this case, the amplitude and width of the IDP is varied for two electron temperatures, that is,  $T_e = 4T_i$  and  $10T_i$ . The Run-12 marked in bold as its output is saved at very high time resolution to examine the ponderomotive processes during evolution of IASWs.

Run	$T_e$ [ $T_i$ ]	$V_{th e}$ [ $V_{th i}$ ]	$dx$ [ $\lambda_{di}$ ]	$dt$ [ $\omega_{pi}^{-1}$ ]	$L_x$ [ $\lambda_{di}$ ]	$l_0$ [ $\lambda_{di}$ ]	$\Delta n$ [ $n_0$ ]	$t_S$ [ $\omega_{pi}^{-1}$ ]	$t_B$ [ $\omega_{pi}^{-1}$ ]	$N_{sol}$
7	4	20	0.4	0.001	$3 \times 10^5$	150	0.5	296	528	8
8	4	20	0.4	0.001	$3 \times 10^5$	150	0.6	280	440	9
9	4	20	0.4	0.001	$3 \times 10^5$	150	0.75	264	360	10
10	4	20	0.4	0.001	$3 \times 10^5$	150	0.9	242	312	11
11	4	20	0.4	0.001	$4 \times 10^5$	150	1.0	240	288	12
<b>12</b>	<b>4</b>	<b>20</b>	<b>0.4</b>	<b>0.001</b>	<b><math>3 \times 10^5</math></b>	<b>100</b>	<b>0.5</b>	<b>172</b>	<b>350</b>	<b>6</b>
13	4	20	0.4	0.001	$3 \times 10^5$	125	0.5	240	440	7
7	4	20	0.4	0.001	$3 \times 10^5$	150	0.5	296	528	8
14	4	20	0.4	0.001	$3 \times 10^5$	175	0.5	376	620	9
15	4	20	0.4	0.001	$3 \times 10^5$	200	0.5	464	696	10
16	10	31.6	0.4	0.001	$3 \times 10^5$	150	0.5	168	355	5
17	10	31.6	0.4	0.001	$3 \times 10^5$	150	0.6	149	293	6
18	10	31.6	0.4	0.001	$3 \times 10^5$	150	0.75	138	230	7
19	10	31.6	0.4	0.001	$3 \times 10^5$	150	0.9	130	202	7
20	10	31.6	0.4	0.001	$4 \times 10^5$	150	1.0	125	187	8
21	10	31.6	0.4	0.001	$3 \times 10^5$	100	0.5	76.8	230	4
22	10	31.6	0.4	0.001	$3 \times 10^5$	125	0.5	110	314	5
16	10	31.6	0.4	0.001	$3 \times 10^5$	150	0.5	168	355	5
23	10	31.6	0.4	0.001	$3 \times 10^5$	175	0.5	197	422	6
24	10	31.6	0.4	0.001	$3 \times 10^5$	200	0.5	245	475	7

ions and is called the electron plasma wave or Langmuir wave. The low-frequency waves are the ion acoustic waves that are longitudinal density perturbations, driven by the electric field that arises from the space charge developed by the slight displacement between ion and electron density perturbations in the simulation. Since the ions and electrons oscillate in phase, the ion space charge, which would normally tend to push the ion compressions apart, is neutralized or shielded by the electrons. However, due to their thermal motion, some electrons overshoot the ion charge clouds; hence, the shielding is incomplete and an electric field is developed which then drives the IA waves in space.

Here, we discuss the generation and evolution of the IA solitons through wave breaking process. The schematics of the different steps involved in the evolution of the IA solitons through wave breaking process is shown in Figure 1. The electron and ion equilibrium densities  $n_j(x)$  in the system is subjected to the long wavelength IDP at  $\omega_{pi}t = 0$  as shown in Figure 1(a). Here,  $t$  is a product of the number of simulation time steps  $\Delta t$ . The introduction of the IDP causes a charge separation in the plasma. This charge separation creates finite electrostatic potential  $\phi$  in the system. We show the evolution of the electrostatic potential at different stages of the simulation in the other panels of Figure 1.

First, we observe the formation of the trough at the top of the electrostatic potential pulse in the early stage of the simulation at  $\omega_{pi}t = t_1$ , which is shown in Figure 1(b). The center of the trough oscillates with time to form Langmuir modes, which are preceded by the IA solitary pulses formed through splitting of this potential structure as shown in Figure 1(c) at  $\omega_{pi}t = t_2$ . Both IA solitary pulses are found to be weakly nonlinear and has longer wavelengths. The IA solitary pulses and the Langmuir wave packets are indistinguishable and propagate towards the opposite boundaries of the simulation system with time. The Langmuir wave packets propagate with the group velocity ( $V_g$ ) greater than the phase speed of IASWs. Later, during their propagation the amplitude and speed of IA pulses gradually increases. Consequently, the trailing edges of both pulses tend to steepen at time  $\omega_{pi}t = t_3$ . One of such pulse is shown in Figure 1(d). Because of the steepening, the long wavelength IA solitary potential pulse amplitude increases. Further both pulses collapse through the wave breaking process at  $\omega_{pi}t = t_4$  as depicted in the Figure 1(e). Once initiated, the wave breaking process continues till the formation of two chains of unstable short wavelength IASW pulses. One chain of such unstable IASW pulses propagating towards the right-side boundary of the simulation system at time  $\omega_{pi}t = t_5$  is shown in the Figure 1(f). The unstable IASW pulses in these chains eventually evolved into the stable IA solitons after a sufficiently long time. The details of different simulation runs are given in Tables I and II.

In order to have better understanding of the generation, steepening and breaking process of IASWs, we have studied the plasma and IASWs characteristics for Run-12 ( $l_0 = 100\lambda_{di}$ ,  $\Delta n = 0.5n_0$ ,  $T_e = 4T_i$ ), where we have taken the simulation output at a very high time resolution, that is, at every  $\omega_{pi}t = 0.005$ . This simulation run is marked in bold in Table II and discussed here in detail. We examined the time

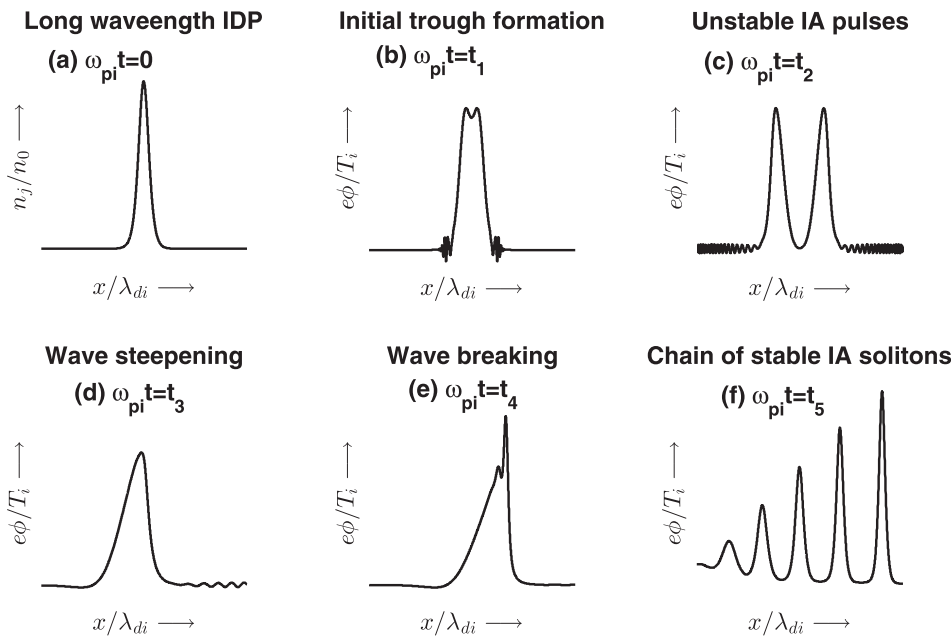


FIG. 1. Schematic diagrams illustrate some of the stages during formation and evolution of chains of multiple IA solitons in the simulation. (a) The perturbed densities  $n_j(x)$  in the simulation at  $\omega_{pi}t=0$ . (b) The perturbations introduce the finite electrostatic potential in the system. The formation of trough observed at the top of this potential pulse at  $\omega_{pi}t_1$ . At this time, the Langmuir oscillations also evolved at both sides of the potential pulse. (c) Two long wavelength IASW pulses along with the Langmuir wave packets are formed in the system at  $\omega_{pi}t_2$ . (d) The trailing edge of both IASW pulses steepens at  $\omega_{pi}t_3$ . One of such pulse is shown in this panel. (e) After steepening, the IASW pulse breaks at  $\omega_{pi}t_4$ . At this stage, the short wavelength pulses steepens at the topside of the IASW pulses. (f) The short wavelength pulses later evolved into chains of IA solitons in the system.

variation of various physical parameters like peak electron, ion velocities ( $v_{emax}$ ,  $v_{imax}$ ), maximum kinetic energy of electron ( $KE_{emax}$ ), maximum potential energy ( $U_{max}$ ), peak electron, ion densities ( $n_{emax}$ ,  $n_{imax}$ ), and IA pulse phase speed ( $V_s$ ). We compute the electrostatic and kinetic energy per unit volume using  $U = \epsilon E^2/2$  and  $KE_s = n_s m_s v_s^2/2$ , respectively. These parameters are estimated for Run-12 and shown in Figures 2(a)–2(d). Four vertical black dotted lines plotted in Figure 2 corresponds to time  $t_1$ ,  $t_2$ ,  $t_3$ , and  $t_4$  associated with different stages during the generation and evolution of IASWs as described in schematic shown in Figures

1(b)–1(e). These stages are identified based on the time evolution of the potential structure and other physical parameters of the simulation system.

Time  $t_1$  represents the stage where top of potential structure is plunged into the trough in the early phase of the generation process. It is found that the lighter species, that is, electron initially gains momentum, whereas the ions remain stationary. The maximum velocity of the electrons oscillate and increase rapidly, whereas, the maximum velocity of the ions increase slowly. The progression of the maximum velocity of the electrons indicates that the electrons quickly respond to the IDP

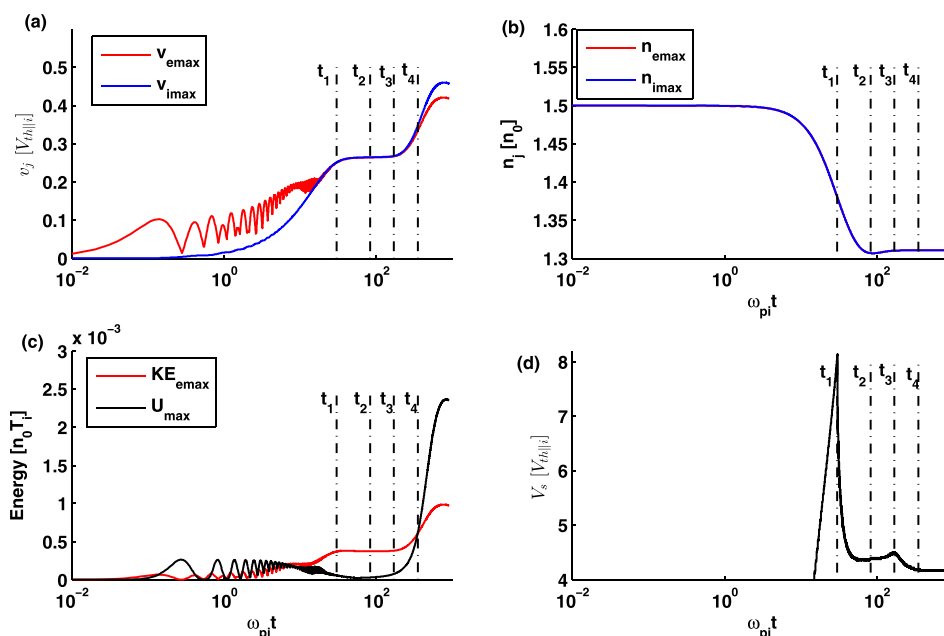


FIG. 2. Variation of (a) electron and ion maximum velocities, (b) electron ion maximum densities, (c) maximum electrostatic energy ( $U_{max}$ ), and the maximum kinetic energy of the electrons ( $KE_{emax}$ ), (d) The phase speed of the IASW pulse as a function of time for the simulation Run-12. The vertical lines in the panels at time  $t_1$ ,  $t_2$ ,  $t_3$ , and  $t_4$  represent different evolutionary stages of IASWs as mentioned in Figure 1.

in the system because of their lighter mass. However, massive ions respond slowly as evident in Figure 2(a). Also, the maximum kinetic energy of electron is found to be smaller compared to the maximum potential energy. Later, it exceeds the maximum potential energy as electron gains momentum in the early phase of development ( $<t_1$ ) as seen in Figure 2(c). So either potential or fluid velocities can be used to get the estimates of  $t_1$ .

The time  $t_2$  represents the stage where initial potential pulse splits and two IASW pulses are generated. Other physical parameters do not show any peculiar feature at this time, and hence, it can be determined using the time evolution of potential structures. It should be noted that from time  $t_2 = 83\omega_{pi}^{-1}$  the phase speed of IASW pulse increases and attains peak at time  $t_3$ , which is identified as the start of the steepening process (see Figure 2(d)). The electron and ion velocities are nearly same and remain unchanged from  $t_1 = 30\omega_{pi}^{-1}$  till time  $t_3 = 170\omega_{pi}^{-1}$ . The maximum electrostatic energy gradually start to increase from time  $t_3$  and it exceeds the maximum kinetic energy of electron at time  $t_4 = 350\omega_{pi}^{-1}$  (see Figure 2(c)). This take over time is identified as breaking time of IASW pulse. Thus, monitoring the time evolution of maximum ion-electron velocities, potential, phase speed of IA pulse, maximum electron kinetic energy, and the maximum potential energy in the simulation system, one can get the estimates of time corresponding to different evolutionary stages of IASWs in plasma. As the time of the initiation of different stages during the generation and wave breaking of IASWs have been identified, we now examine the ponderomotive processes that are discussed in Sec. IV.

#### IV. ESTIMATE OF PONDEROMOTIVE PROCESSES

We initialize the fluid simulation by introducing the IDP in the equilibrium electron and ion densities as discussed in Sec. III. It is seen that the electrons quickly respond to the perturbation and the finite electric field developed in the system. When such spatially varying electric field is present in the system, the electrons and ions experience the ponderomotive force ( $F_p$ ). In one-dimension (along- $x$ ), the ponderomotive force experienced by the electrons due to the non-uniform electric field oscillating at frequency  $\Omega$ , that is,  $E(x, t) = E_0(x) \cos(\Omega t)$  is given by

$$F_p = -\frac{e^2}{4m_e\Omega^2} \frac{\partial}{\partial x} |E|^2 = -e\nabla\Psi. \quad (7)$$

Here, ponderomotive potential  $\Psi$  is given by following equation,

$$\Psi = \frac{1}{4} \frac{e}{m_e\Omega^2} |E|^2 = \frac{1}{2} \frac{e}{\varepsilon_0 m_e \Omega^2} U. \quad (8)$$

In the equations above,  $e$  is the electrical charge of the electron,  $m_e$  is its mass,  $\Omega$  is the angular frequency of oscillation of the field,  $E$  is the amplitude of the electric field,  $\Psi$  is the ponderomotive potential, and  $U$  is electrostatic energy. This force is much stronger for electrons than ions, owing to the inverse dependence on mass in the above Equation (7). It should be noted that while computing ponderomotive potential

using Equation (8) we need the estimates of ponderomotive frequency. Using above Equation (7), we derived the expression for ponderomotive frequency  $\Omega$  as follows:

$$\Omega^2 = \frac{U}{KE_e} \frac{\omega_{pe}^2}{4}, \quad (9)$$

where  $KE_e$  is the electron kinetic energy. Similar equations can be obtained for ion as well. To understand the breaking of the IASWs, we followed the maximum electrostatic potential, maximum ponderomotive potential associated with the electrons and the ions in the simulation system. These physical quantities are, respectively, shown in Figures 3(a), 3(c), and 3(e) with their spectrogram in Figures 3(b), 3(d), and 3(f). The vertical (horizontal) dotted lines in the left (right) panel of Figure 3 represent time  $t_1$ ,  $t_2$ ,  $t_3$ , and  $t_4$ . Apart from the ponderomotive potential, here, we examine the time variation of maximum electrostatic potential, as in many of the earlier studies the wave breaking limit is proposed based on this parameter. Figure 3(a) shows the time evolution of the maximum electrostatic potential for Run-12. We also have obtained the power spectrogram of the maximum electrostatic potential in the system, which is depicted in Figure 3(b). The spectrogram shows presence of both ion acoustic ( $\omega_{pi} = 1$ ) and Langmuir ( $\omega_{pe} = 10$ ) modes. It is evident that, the ion acoustic mode has higher power throughout the spectrogram, whereas power in the Langmuir mode decreases with the time. The spectrogram shows that Langmuir mode loses energy during the process of generation of IASWs, and hence, becomes weaker after time  $t_2$ .

Both electron and ion ponderomotive potentials show similar trend at the different stages involved during the generation and evolution of IASWs. It is seen that both  $\Psi_e$  and  $\Psi_i$  gradually increased with time, and later attains maximum at time  $\approx t_1$ . After this maxima, both ponderomotive potentials in the system start decreasing, and reach minimum at time  $\approx t_2$ . After this step, both electron and ion ponderomotive potential in the system increase during the steepening of the IASW pulse and attains maximum at time  $\approx t_4$ , that is, IASW breaking time. The frequency spectrogram of the maximum ponderomotive potential of the electrons and ions are shown, respectively, in Figures 3(d) and 3(f). Both spectrograms show the ion acoustic mode and the Langmuir mode. The harmonics of the Langmuir modes can be seen at the multiple of Langmuir frequency. It is seen that the Langmuir mode loses most of its energy during the generation of the IASWs. The most interesting feature of Figure 3 is that the time of IASW breaking coincides with the maximum ponderomotive potential rather than the maximum electrostatic potential, as suggested by some of the earlier studies.

Furthermore, we investigate the time evolution of the average ponderomotive frequencies of the electrons and ions, which is shown in Figure 4. The lower and upper blue dashed horizontal lines show the ion plasma frequency ( $\omega_{pi}$ ) and electron plasma frequency ( $\omega_{pe}$ ), respectively. This figure shows that the average ponderomotive frequencies, both ions and electrons, initially, have larger amplitudes. It is observed that electron (ion) average ponderomotive frequency approaches the frequency smaller than electron (ion) plasma frequency

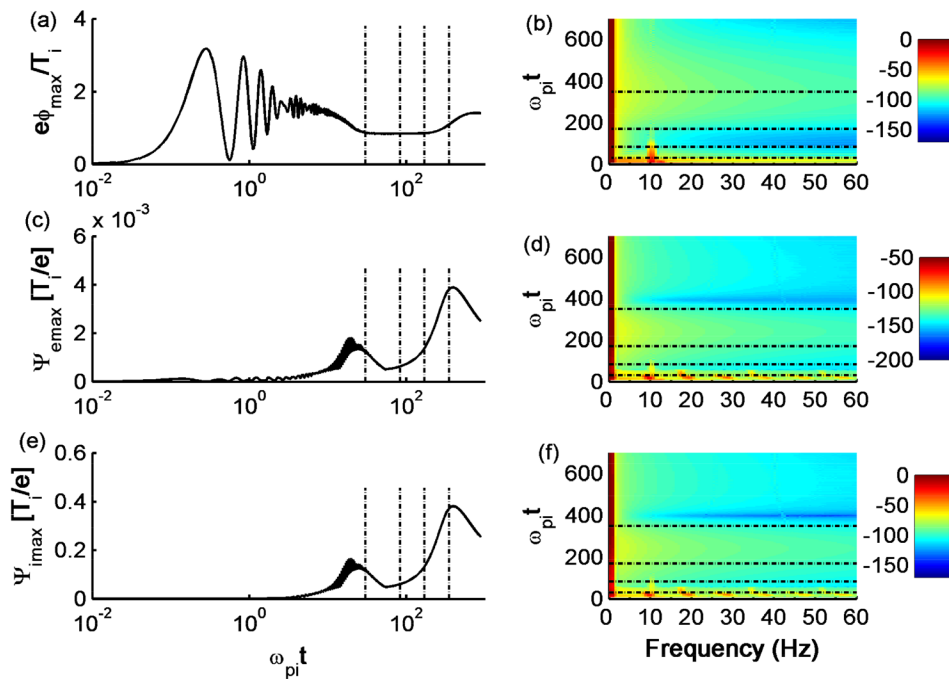


FIG. 3. Time variation of maximum (a) electrostatic potential (c) electron ponderomotive potential (e) ion ponderomotive potential with their corresponding spectrogram, respectively, shown in (b), (d) and (f) for Run-12. The vertical and horizontal lines in the left and right panels show time  $t_1$ ,  $t_2$ ,  $t_3$ ,  $t_4$ , which represent different evolutionary stages of IASWs as mentioned in Figure 1.

at the time ( $t_1$ ). These frequencies remain unchanged from time  $t_1$  to  $t_3$ , that is, till the initiation of the steepening of IASW pulse. The average ponderomotive frequencies start increasing gradually during the steepening and breaking of IASWs. The variation of the ponderomotive potentials and the ponderomotive frequencies of the electrons and ions during various stages in the simulation indicate that the ponderomotive processes play an important role in the breaking of IASWs.

## V. ELECTRON TEMPERATURE EFFECT ON THE STEEPENING AND BREAKING OF THE IASWs

We perform six simulation runs for different electron temperatures  $T_e = 4T_i$  (Run-1),  $6T_i$  (Run-2),  $8T_i$  (Run-3),

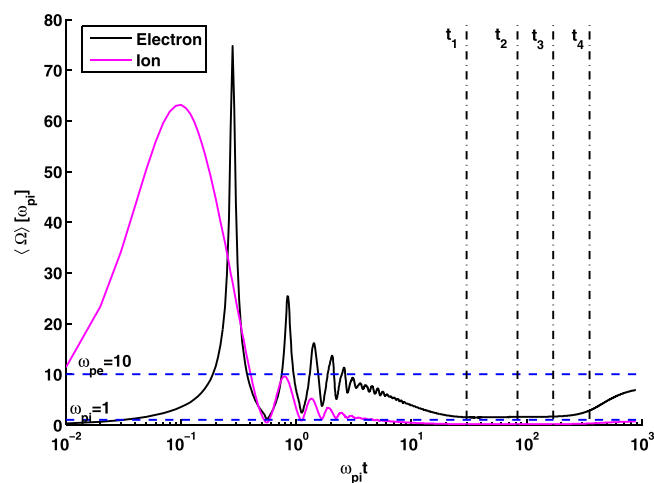


FIG. 4. Time evolution of the average ponderomotive frequency of the electrons and ions estimated for Run-12. The lower and upper blue dashed horizontal lines show the ion plasma frequency ( $\omega_{pi}$ ) and electron plasma frequency ( $\omega_{pe}$ ), respectively. The vertical lines in the panels at time  $t_1$ ,  $t_2$ ,  $t_3$ , and  $t_4$  represent different evolutionary stages of IASWs as mentioned in Figure 1.

$10T_i$  (Run-4),  $12T_i$  (Run-5), and  $15T_i$  (Run-6), which corresponds to the electron thermal speed ( $V_{th|e}$ ) of 20, 24.5, 28.3, 31.6, 34.6 and 38.7, respectively, in the units of ion thermal speed ( $V_{th|i}$ ). The IDP parameters  $l_o$  and  $\Delta n$  are taken as  $150\lambda_{di}$  and  $0.5n_0$ , respectively, for all these runs. We took grid spacing  $\Delta x = 0.4\lambda_{di}$ , and system length  $L_x = 6 \times 10^4 \lambda_{di}$  for all the fluid simulation runs. The time interval  $\Delta t$  for each run is chosen such that the numerical speed  $\Delta x/\Delta t$  larger than the maximum speed in the system (i.e.,  $V_{th|e}$  in our model). All the parameters of these simulation runs are given in Table I. Among these runs, we compare the occurrence of various stages involved in the course of evolution of IA solitons in the simulation systems with two different temperature.

Figure 5 shows different stages during the generation and evolution of IASWs that are discussed in previous sections for (a) Run-1 ( $T_e = 4T_i$ , i.e.,  $V_{th|e} = 20.00 V_{th|i}$ ), and (b) Run-4 ( $T_e = 10T_i$ , that is,  $V_{th|e} = 31.62 V_{th|i}$ ). Although, we used same IDPs in the electron and ion equilibrium densities  $n_j(x)$  in both simulation runs at  $\omega_{pit} = 0$ ; there are several differences in the evolution of IASWs. As discussed in the Figure 1, injecting the IDP in the equilibrium densities of the electrons and ion, evolved the IA solitons and Langmuir wave packets in both simulation runs. The evolution of IA solitons involve formation of the trough, formation of long wavelength IASW pulses along with the Langmuir wave packets, steepening and breaking of the IASW pulses in both simulations run, which are shown separately in Figures 5(a) and 5(b). From this figure, it is observed that the IASW pulse steepens at time  $\omega_{pitS} = 296$  for the simulation Run-1, whereas it occur at time  $\omega_{pitS} = 173$  in the simulation Run-4. The breaking of IASW pulse initiates early for the simulation Run-4 (at  $\omega_{pitB} = 355$ ) as compared to the Run-1 (at  $\omega_{pitB} = 528$ ). We observed five number of IA solitons in the simulation system for Run-4, whereas the simulation Run-1 evolved seven number of solitons in the system as shown in

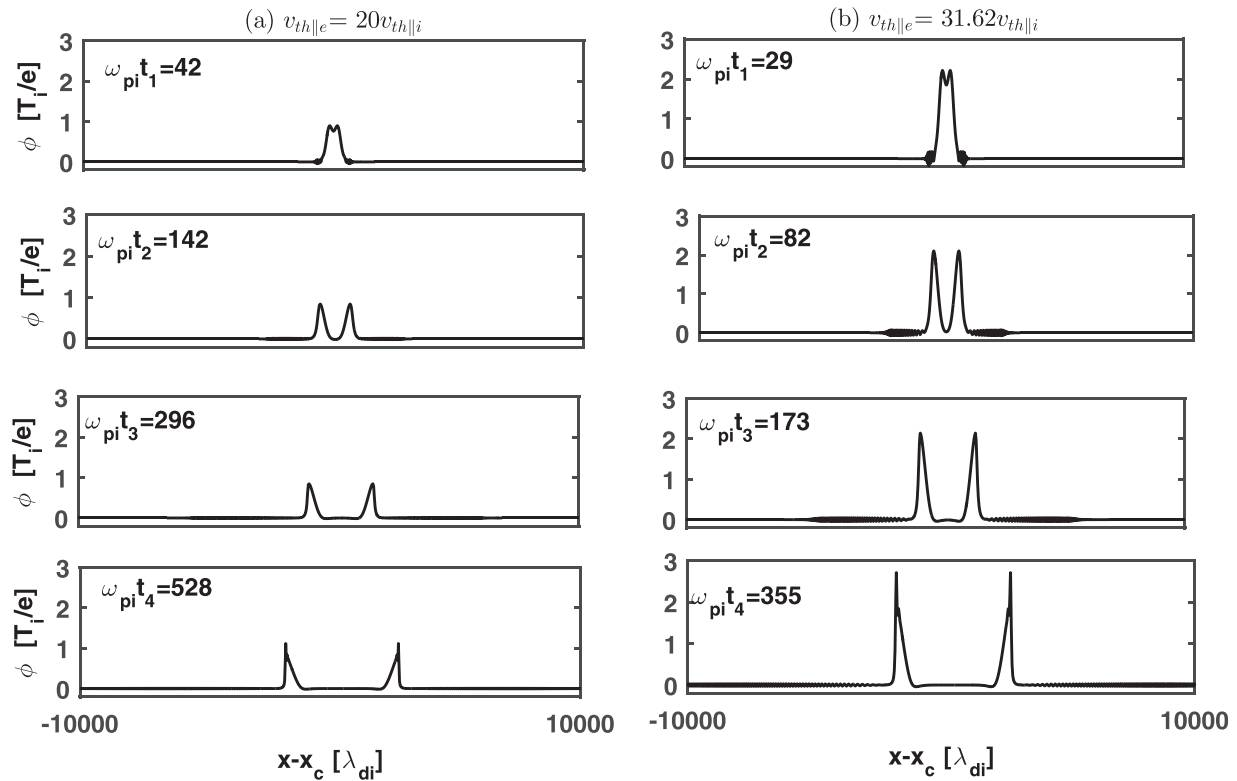


FIG. 5. The profiles of potential for (a) Run-1 and (b) Run-2 at time  $t_1$ ,  $t_2$ ,  $t_3$ , and  $t_4$  that corresponds to different evolutionary stages of IASWs as mentioned in Figure 1. The top panels show formation of trough at the point top of potential pulse along with the Langmuir oscillations at the endpoints of the potential pulse at  $\omega_{pi}t = 42$  in Run-1, and at  $\omega_{pi}t = 29$  in Run-4. Later, two IASW pulses along with two Langmuir wave packets are evolved in the simulation Run-1 at time  $\omega_{pi}t = 142$ , and in the simulation Run-4 at time  $\omega_{pi}t = 82$ . The IASW pulses in the simulation Run-1 and Run-2 steepens at time  $\omega_{pi}t = 296$  and  $\omega_{pi}t = 173$ , respectively. After gaining the larger amplitude, the IASW pulse in Run-1 breaks at time  $\omega_{pi}t = 522$  and in Run-4 at time  $\omega_{pi}t = 355$ .

the Figure 6. The amplitudes of IASW pulses and Langmuir wave packets in the Run-4 are larger than those are observed in the Run-1. Furthermore, it is seen that the IA solitons in both simulation runs support bipolar electric field structures as shown in Figures 6(c) and 6(d). The electric field amplitude of the IA solitons in Run-4 is larger as compared to the amplitude of the solitons in Run-1.

The time of steepening and breaking of IASWs are determined from time variation of the phase speed and the energies for each simulation run. Figure 7(a) shows the variation of phase speed of the IASW pulse with time for Run-1 (blue curve) and Run-4 (red curve). This figure shows two peaks in the IASW pulse phase speed corresponding to two different electron temperatures. In both runs, the first peak of the phase speed of the pulse is close to the time of the initiation of the trough formation at the point top of the initial potential pulse. Whereas the second peak (shown with the vertical dashed lines) is at the time of the steepening of the IASW pulse. It is seen that the steepening occurs early in simulation Run-4 than in simulation Run-2. The time variation of the maximum electrostatic energy and the electron kinetic energy for Run-1 (blue curves) and Run-4 (red curves) are shown in Figure 7(b). As mentioned earlier, the wave breaking initiates at the time where the maximum potential energy takes over the maximum kinetic energy of the electrons in the system. With this criteria of the wave breaking, it is seen that the wave breaking initiates early in Run-4 (at  $\omega_{pi}t_B = 355$ ) compared to Run-1 (at  $\omega_{pi}t_B = 528$ ).

The breaking time in both runs are shown with the vertical dashed lines in Figure 7(b).

We have computed start time of the steepening ( $t_S$ ) and breaking ( $t_B$ ) of the IASW for the simulation runs with different temperature as given in Table I. Figure 8 shows the start time of the IASW steepening ( $t_S$ ) and breaking ( $t_B$ ) as a function of electron thermal velocity in the system. It should be noted that the long wavelength IDPs used to perturb the equilibrium ion and electron densities for simulation Run-1 to 6 are same. It is evident that the onset time of the steepening and breaking of the IASW is inversely proportional to the electron thermal velocity. We have also observed that the number of solitons formed in the chain depends on the electron thermal velocity. The number of solitons in the chain for each simulation run are mentioned in Table I.

## VI. IDP CHARACTERISTICS EFFECT ON THE STEEPENING AND BREAKING OF THE IASWS

In this section, we discuss the role of amplitude and width of the IDP in the evolution of the IASWs for two different electron temperatures. Here, we use the simulation runs from Table II, where amplitude and width of the IDPs are considered as  $\Delta n = 0.5, 0.6, 0.75, 0.9, 1$  in the units of  $n_0$ , and  $l_0 = 100, 125, 150, 175, 200$  in the units of  $\lambda_{di}$ , respectively. For each combination of these parameters, the simulation runs are taken for two electron temperatures

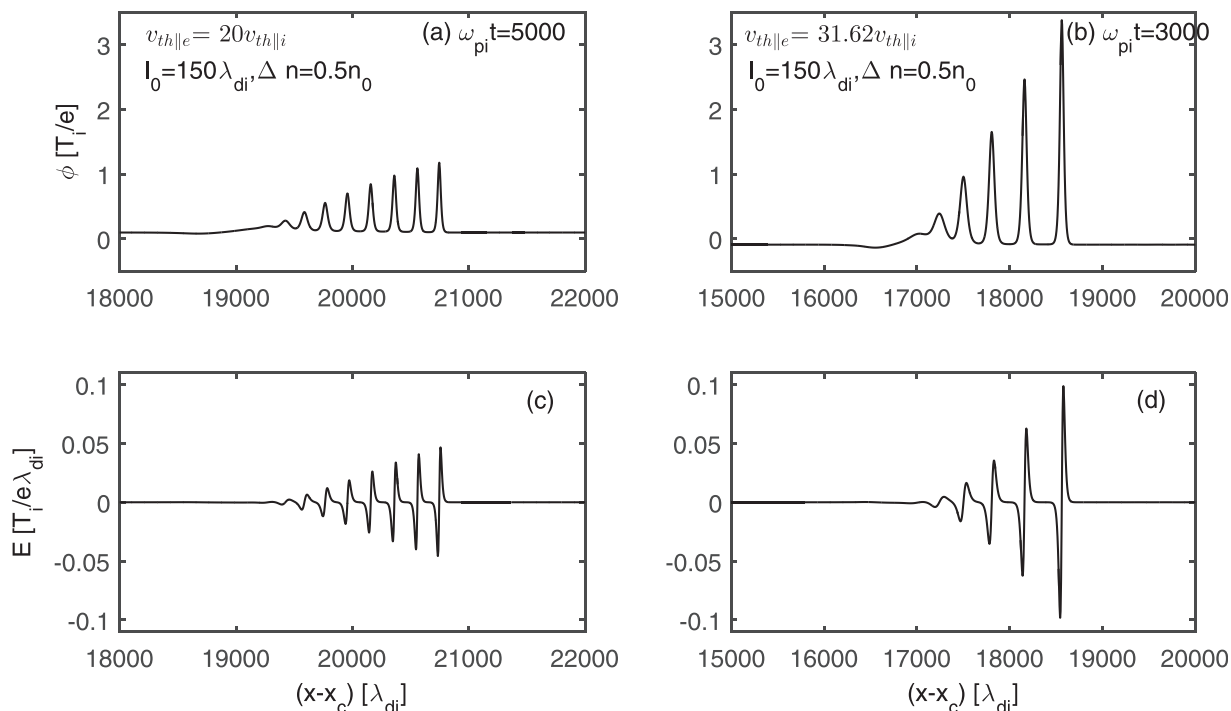


FIG. 6. Snapshots of the electrostatic potential of the short wavelength IASW pulses in the chain for the simulation runs (a) Run-1, and (b) Run-4. The electric field associated with the IASW pulses in the chain is shown in the panel (c) and (d), respectively, for the Run-1 and Run-4. The profiles shown here are associated with the solitary pulses propagating in positive  $x$ -direction.

$T_e = 4T_i$  and  $T_e = 10T_i$ . The fluid simulation parameters along with the onset time of the steepening and breaking of the IASW, and the number of stable solitons formed in the IA chain in each simulation runs are listed in Table II. The simulation runs 7–15 and 16–24, respectively, represent the electron temperature  $T_e = 4T_i$ , that is,  $V_{th||e} = 20.00V_{th||i}$  and  $T_e = 10T_i$ , that is,  $V_{th||e} = 31.62V_{th||i}$ . Using the criteria for identifying the initiation of the steepening and the breaking of the IASW as discussed in Sec. V, we have obtained the time of the initiation of the steepening and breaking of the IASW for each simulation run. Figure 9(a), shows the onset time of the breaking of the IASW (upper panel), and steepening (lower panel) for different amplitude of the IDP. In Figure 9(b), the start time of the IASW breaking (upper

panel), and steepening (lower panel) are plotted as a function of the IDP width  $l_0$ . It is found that the start time of the breaking and steepening of the IASW decreases with the increase of IDP amplitude  $\Delta n$ , in case of both electron temperatures. Whereas, it increase with the increase of IDP width (see Table II). Thus, we find that steepening and breaking time is proportional to  $l_0/\Delta n$ . The number of IA solitons in the chain is found to increase with increase of both amplitude and width of IDP.

It is evident that the amplitude and width of the IDP play an important role in determining the steepening and breaking time of the IASWs in plasma. Kakad *et al.*<sup>10</sup> have shown that the power associated with the IDP in  $k$ -space is important, and it decides the long- or short wavelength criteria for the

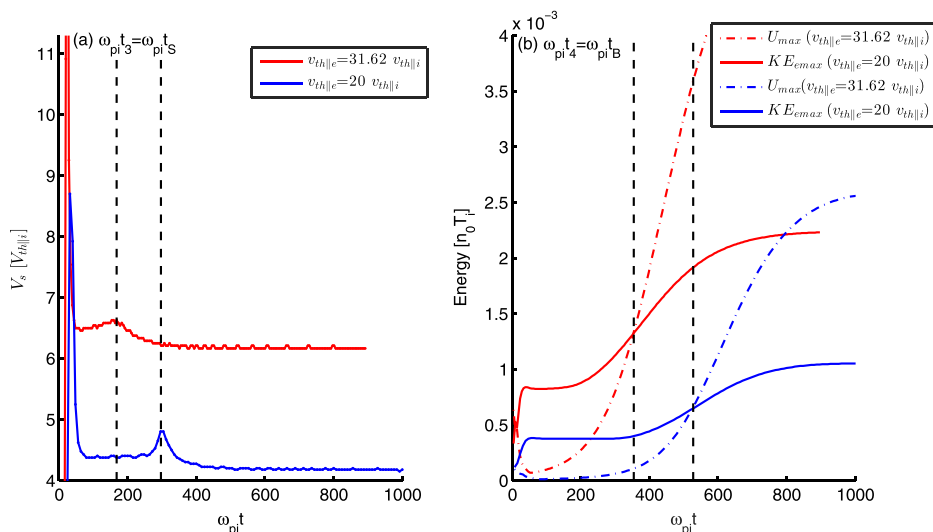


FIG. 7. (a) The variation of the phase speed ( $V_s$ ) of the IASW pulse with time for Run-1 ( $T_e = 4T_i$ ,  $V_{th||e} = 20.00 V_{th||i}$ ) and Run-4 ( $T_e = 10T_i$ ,  $V_{th||e} = 31.62 V_{th||i}$ ). The vertical lines indicate the time of maximum phase speed of IASW pulse after their formation and is defined as the their steepening time. (b) Time evolution of the electrostatic energy ( $U$ ) and the maximum kinetic energy of the electrons ( $KE_{max}$ ) for the simulation Run-1 and Run-4. Vertical lines show the time when maximum electrostatic energy exceeds the maximum electron kinetic energy, which is defined as the breaking time for IASWs.

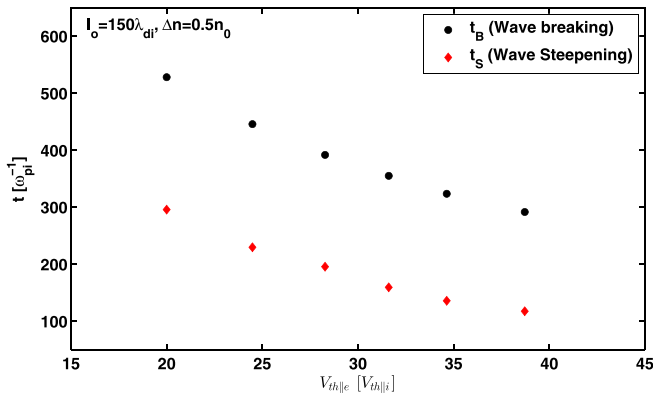


FIG. 8. The start time of the steepening ( $t_S$ ) and breaking ( $t_B$ ) of the IASW pulse as function of electron thermal velocity,  $V_{th||e}$ . We fixed the IDP amplitude  $\Delta n = 0.5n_0$  and width  $l_0 = 150\lambda_{di}$  for these simulation runs.

IDP. In both long- and short wavelength IDP causes simulation system to evolve in different ways. Thus, we estimated the average power of IDP in  $x$ - and  $k$ -space to understand the IDP dependence of IASW breaking time. We have  $\delta n = \Delta n \operatorname{sech}^2(x/l_0)$ . Let us assume,  $f(x) = \delta n$ . Thus, the perturbation in  $k$ -space becomes  $f(k) = \pi \Delta n l_0^2 k \operatorname{cosech}(k\pi l_0/2)$ . The average power associated with the IDP in  $x$ - and  $k$ -space, respectively, take the form  $\langle f(x) \rangle = 2\Delta n l_0$  and  $\langle f(k) \rangle = 2\pi\Delta n$ . Thus, we find that the quantity  $\langle f(x) \rangle / [\langle f(k) \rangle]^2$  is proportional to  $l_0/\Delta n$ . Thus, the average power of IDP in space and frequency domain determines the breaking time of IASWs.

### VII. SUMMARY AND CONCLUSIONS

We have performed one-dimensional fluid simulations to investigate the steepening and breaking of the IASWs in plasma by considering the long wavelength IDP. We have adopted the wave breaking terminology from the past research articles.<sup>7,9,10,18</sup> This terminology is identical to

those of splitting or disintegration of the wave pulse in plasma. To some extent, this is also likens to the breaking of surfer’s crest/wave near the coast, in which pre-breaking region of the wave transformation is described by the effects of wave steepness due to the nonlinearity (or amplitude dispersion) and wave shortness due to the frequency dispersion. In this case, the bathymetric variations in shallow water distort this balance, which cause instabilities and subsequent wave breaking. The disintegration of the initially developed long-wavelength weakly dispersive solitary pulse in the present plasma simulation breaks in nearly the same manner. In the pre-breaking region, the long wavelength solitary wave transformation occurs by the effects of the wave steepness due to the nonlinearity. However, the wave breaks due to the lack of dispersive effects required for balancing the nonlinear effects in the system.

We find that the IDP in the plasma initially evolves into the long wavelength IASWs and Langmuir waves. Later, the simulation shows that the long wavelength IASWs steepen, breaks and evolves into the chain of stable IA solitons and the IA oscillations in the system. We have discussed the generation of nonlinear IA solitons through breaking of the long wavelength IASWs, with a particular emphasis placed on the criteria of wave steepening, wave breaking and beyond breaking of the waves. We have examined the ponderomotive processes during the generation and evolution of IASWs.

The fluid simulation performed in this paper established the conditions for steepening and breaking of the IASWs in terms of the (a) maximum phase speed of IASW pulse and (b) balance between maximum electron kinetic energy and the maximum potential energy. Our simulation shows that the conditions for the steepening and breaking of the IASWs can be inventoried by tracking these quantities from the simulation. It is found that the steepening of the IASW initiates when the IASW pulse accelerate and attains the peak after

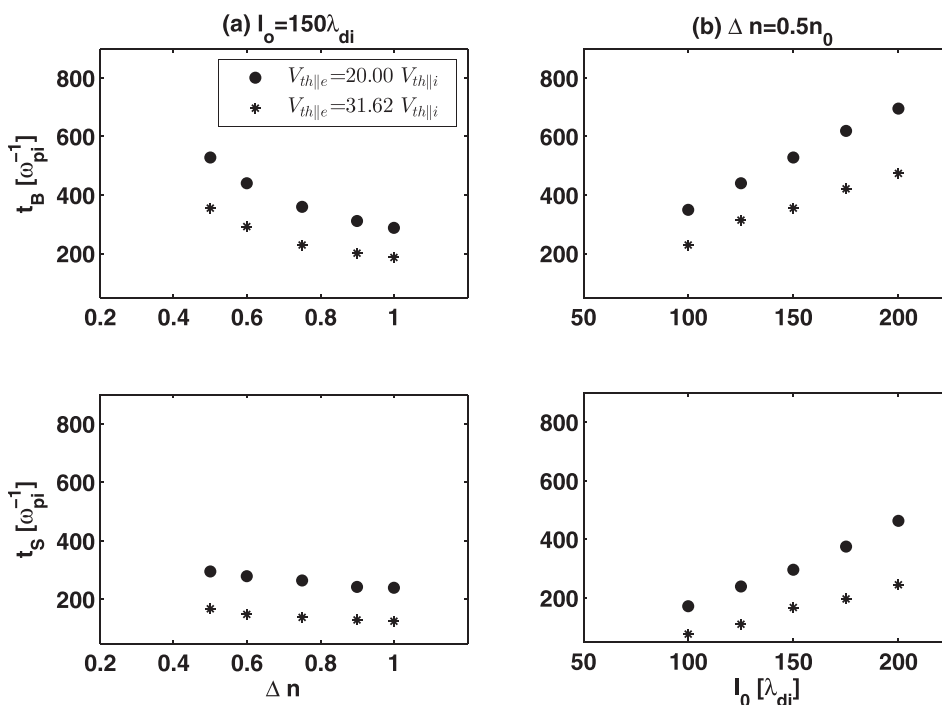


FIG. 9. (a) Start time of the breaking (upper panel) and steepening (lower panel) of the IASW as a function of IDP amplitude  $\Delta n$  for  $V_{th||e} = 20 V_{th||i}$  and  $31.62 V_{th||i}$ . Here, the IDP width,  $l_0 = 150\lambda_{di}$ . (b) The start time of the breaking (upper panel) and steepening (lower panel) of the IASW as function of IDP width  $l_0$  for  $V_{th||e} = 20 V_{th||i}$  and  $31.62 V_{th||i}$ . Here the IDP amplitude,  $\Delta n = 0.5n_0$ .

their generation. Whereas, the breaking of the IASWs initiates when the maximum potential energy in the system takes over the maximum kinetic energy of the electrons.

Our simulation demonstrates the nature of the ponderomotive potentials and ponderomotive frequencies of the electrons and ions in the course of evolution of IASWs in plasma. Both electron and ion ponderomotive potentials attain first maxima at the formation of the trough at the point top of the initially generated potential structure, and the second maxima at the time of the initiation of the breaking of the weakly nonlinear long wavelength IASWs. In addition, it is noticed that, the electron (ion) ponderomotive frequency initially has amplitude greater than the electron plasma frequency, which quickly reduce and becomes smaller than electron (ion) plasma frequency in the generation process of the IASWs in the system. Both ponderomotive frequencies of the electrons and ions remains unchanged from the time of formation of the IA waves up to the time of the initiation of the steepening of the IASWs. Later, during steepening of the IASWs, the electron and ion ponderomotive frequencies found to increase slowly. Based on this, we proposed that the characteristics of electron and ion ponderomotive potentials and the ponderomotive frequencies can be used as proxies to determine the steepening and breaking time of the IASWs.

Understanding the wave behavior during its breaking is important for many practical applications ranging from particle acceleration to plasma heating. It is noted that the nonlinear effects in plasma limit the amplitude of the generated waves. The results presented in this paper indicate that the electron thermal velocity, the IDP width and the IDP amplitude determine the time of generation, steepening and breaking of the IASWs. The wave breaking occurs early for the larger electron temperature plasma in comparison with the lower electron temperature. For the fixed perturbation width, the wave breaking occurs earlier for the larger density perturbations. However, for the fixed density perturbations, the breaking occurs at earlier time for the smaller width perturbations. The breaking of the IASWs enhances the dispersive effects through development of the short wavelength IASW pulses in the system. After a long time, the dispersion in the IASW counter balanced by nonlinearity, and the formation of chains of IA solitons take place. The number of solitons and their characteristics depends on the electron temperature, width, and amplitude of the IDP. The dependence of the

IASW steepening and breaking time on the IDP characteristics like width and amplitude can be understood based on the average power of IDP in space and frequency domain.

## ACKNOWLEDGMENTS

The model computations were performed on the High Performance Computing System at the Indian Institute of Geomagnetism. Thanks are due to Dr. Yoshiharu Omura, RISH Kyoto University Japan, for his guidance in the development of the fluid code.

<sup>1</sup>J. M. Dawson, *Phys. Rev.* **113**, 383 (1959).

<sup>2</sup>T. P. Coffey, *Phys. Fluids* **14**, 1402 (1971).

<sup>3</sup>W. L. Kruer, *Phys. Fluids* **22**, 1111 (1979).

<sup>4</sup>A. Bergmann and P. Mulser, *Phys. Rev. E* **47**, 3585 (1993).

<sup>5</sup>A. Mukherjee and S. Sengupta, "Breaking of large amplitude electron plasma wave in a maxwellian plasma," preprint [arXiv:1605.05518](https://arxiv.org/abs/1605.05518) (2016).

<sup>6</sup>S. Alikhanov, R. Sagdeev, and P. Chebotaev, "Destruction of a large-amplitude ion-acoustic wave," *Sov. Phys. JETP* **30**, 847 (1970).

<sup>7</sup>C. Judice, J. Decker, and R. Stern, "Breaking and turbulent transition in ion acoustic waves," *Phys. Rev. Lett.* **30**, 267 (1973).

<sup>8</sup>D. Forslund, J. Kindel, K. Lee, and B. Godfrey, "Collapse of very large amplitude ion waves," *Phys. Fluids* **22**, 462 (1979).

<sup>9</sup>P. Rosenau, "Evolution and breaking of ion-acoustic waves," *Phys. Fluids* **31**, 1317–1319 (1988).

<sup>10</sup>A. Kakad, Y. Omura, and B. Kakad, *Phys. Plasmas* **20**, 062103 (2013).

<sup>11</sup>K. Watanabe and T. Sato, "High-precision MHD simulation," *Computer Space Plasma Physics: Simulation Techniques and Software* (Terra Scientific, Tokyo, Japan, 1993), pp. 209–215.

<sup>12</sup>Y. Omura and J. L. Green, "Plasma wave signatures in the magnetotail reconnection region: MHD simulation and ray tracing," *J. Geophys. Res.* **98**, 9189–9199, doi:10.1029/92JA02901 (1993).

<sup>13</sup>B. Kakad, A. Kakad, and Y. Omura, "Nonlinear evolution of ion acoustic solitary waves in space plasmas: Fluid and particle-in-cell simulations," *J. Geophys. Res.* **119**, 5589, doi:10.1002/2014JA019798 (2014).

<sup>14</sup>A. Kakad, B. Kakad, C. Anekallu, G. Lakhina, Y. Omura, and A. Fazakerley, "Slow electrostatic solitary waves in earth's plasma sheet boundary layer," *J. Geophys. Res.* **121**, 4452, doi:10.1002/2016JA022365 (2016).

<sup>15</sup>A. Lotekar, A. Kakad, and B. Kakad, "Fluid simulation of dispersive and nondispersive ion acoustic waves in the presence of superthermal electrons," *Phys. Plasmas* **23**, 102108 (2016).

<sup>16</sup>A. Kakad, A. Lotekar, and B. Kakad, "First-ever model simulation of the new subclass of solitons 'supersolitons' in plasma," *Phys. Plasmas* (unpublished).

<sup>17</sup>A. Lotekar, A. Kakad, and B. Kakad, "Stability and convergence of poisson solver in a fluid plasma simulation with velocity distribution functions," *Phys. Plasmas* (unpublished).

<sup>18</sup>N. J. Zabusky and M. D. Kruskal, "Interaction of 'solitons' in a collisionless plasma and the recurrence of initial states," *Phys. Rev. Lett.* **15**, 240–243 (1965).